Precision Engineering 93 (2025) 481–496

Contents lists available at ScienceDirect

Precision Engineering

journal homepage: www.elsevier.com/locate/precision

Development of a novel self-locking-at-rest piezoelectric inchworm motor with high switching frequency driving ability☆

Sandip Jana [a,b], Sofiane Ghenna [c,d,e], Saikat Kumar Shome [a,b,*], Yves Bernard [d,e], Arup Kumar Nandi [a,b], Laurent Daniel [d,e]

[a] CSIR - Central Mechanical Engineering Research Institute (CSIR-CMERI) Campus, Durgapur, 713209, India
[b] Academy of Scientific and Innovative Research (AcSIR), Ghaziabad, 201002, India
[c] Univ. Polytechnique Hauts-de-France, CNRS, Univ. Lille, Yncrea, Centrale Lille, UMR 8520 - IEMN-DOAE, Valenciennes, F-59313, France
[d] Université Paris-Saclay, Centrale Supélec, CNRS, Laboratoire de Génie Electrique et Electronique de Paris, Gif-sur-Yvette, 91192, France
[e] Sorbonne Université, CNRS, Laboratoire de Génie Electrique et Electronique de Paris, 75252, Paris, France

ARTICLE INFO

Handling Editor: Dr. Masonori Kunieda

Index Terms:
Piezoelectric actuator
Modelling
Inchworm
Sensor
Force measurement

ABSTRACT

In this paper, a novel piezoelectric actuator-based inchworm motor and its driving mechanism has been proposed for high speed linear application. Three high voltage positive square pulses with appropriate phase sequence amongst them have been applied to the two clamps and one extender of IM to achieve the desired linear translation. Isolated mosfet-based switching and oscillation circuits have been designed to operate the motor at high switching frequencies by dynamically reducing the capacitive reactance of the piezoelectric stack actuators. Consequently, experiments on the characterization of the piezo-actuators have been performed to identify the pre stress on the motor rail. Geometric model of the system has been developed using finite element analysis to determine displacement distribution in Clamping Mechanism and Extending Mechanism before physically fabricating the motor prototype to verify the driving mechanism. Performance evaluation has been carried out under varying duty cycles, switching frequencies and loads. The motor is observed to achieve a maximum no load speed of 60 mm/s under the 80–90 V positive square pulse at a frequency of 3 kHz with a 20 % duty cycle. A relatively high electrical driver efficiency of 42 % is experimentally achieved which makes the proposed mechatronic system highly suitable for low-size, high torque industrial applications.

1. Introduction

To improve performance, safety and cost, there has been a radical shift by the original equipment manufacturers for industrial utilities towards automated and enhanced manual control of industrial translation applications [1]. There is an increasing tendency towards rising usage of electrical drive remedies as conventional hydraulic and pneumatic controls are often unsuitable for automatic computer controlled operations due to increased system cost and complexity [2]. Besides, assembly and maintenance of conventional systems also requires extra steps along with additional cabling and connectors. Electromagnetic motors offer an alternative solution with several advantages such as compact size, quick response, high power handling capability, high accuracy, in the field of medical technologies, automotive industries, smart robotic system. However, it requires a number of add-on components, including the control and driver circuit for precise position sensing system.

In contrast, smart actuators over traditional hydraulic and pneumatic cylinders are simpler and smaller installation offer higher power density [3], higher accuracy, less maintenance, less noise [4] and clean environment [5,6]. Therefore smart material based actuators like Piezo-Actuator (PA) are a promising candidate for the development of a new type motor which is a relatively innovative concept [7,8]. PA is a crucial transducer used in micro-nano manipulation with promising application in the area of desktop reconfigurable, biomedical, robotics, vibration control and micro displacement technology [9,10].

☆ Manuscript received Month xx, 2xxx; revised Month xx, xxxx; accepted Month x, xxxx. The authors gratefully acknowledge the funding received from Indo French Center for The Promotion of Advanced Research (IFCPAR/CEFIPRA) for carrying out this work.

* Corresponding author. CSIR - Central Mechanical Engineering Research Institute (CSIR-CMERI) Campus, Durgapur, 713209, India.
E-mail addresses: sandip.cmeri19a@acsir.res.in (S. Jana), Sofiane.Ghenna@uphf.fr (S. Ghenna), saikatkshome@cmeri.res.in (S.K. Shome), yves.bernard@centralesupelec.fr (Y. Bernard), nandi@cmeri.res.in (A.K. Nandi), laurent.daniel@centralesupelec.fr (L. Daniel).

https://doi.org/10.1016/j.precisioneng.2025.01.027
Received 3 October 2024; Received in revised form 31 December 2024; Accepted 30 January 2025
Available online 3 February 2025

Deformable mirrors (DMs) equipped with piezoelectric stacks are extensively used in various wave front control systems, particularly in optical applications requiring high-precision wave front rectification, such as astronomy [11], adaptive optics with bimorph deformable mirror [12], and laser systems [13]. PA commonly arranged in stack configurations, enable rapid and precise adjustments to the mirror surface, hence controlling the radiation wave front and improve laser machining process effectively.

There are several advantages of piezoelectric actuator, like fast transient response characteristics, small size, high electromechanical coupling efficiency, higher blocking force capability to achieve high resolution positioning accuracy. However, practical usage of PA suffers from different kinds of nonlinear phenomena like hysteresis, creep which seriously affects the position and control accuracy [14–17]. Therefore, accurate modeling of the PA is essential towards compensation of the non-linearities.

In the past few years, the inchworm piezoelectric actuator was studied for many applications. This small size motor can be designed for high force or large step displacement and the travel length only depends on slider dimensions. Other advantages are that it is magnetic field free, “high accuracy” and stiffness [18,19].

PA was first introduced for the IM by O’Neill in 1980 to increase the actuation travel range [20] wherein two clamping devices are coupled with cups to actuate them. The idea of linear motion of the piezoelectric inchworm motor(IM) was proposed by Lee et al. using a micro-scale etched electrostatic linear actuator [21,22] which has fast response time and high torque handling capability. Governing design equations for the IM are presented using a system software tool [23].The stiffness interaction between the frame and the PA is key to determining the clamping force and how it affects the positioning [24].

The design and implementation of the driver system of IM is a challenging task due to frequency-dependent capacitive effect of the actuator and presence of existing non-linearities like hysteresis, drift and temperature effects. Table 1 gives the performance overview which is suggestive of a limited range of operating frequency of the inchworm motors. PA displacements are usually within a few tens of micrometers. Several linear IMs have been reported to achieve larger motions [26,27,29,31,33,34,36], though their speed was limited by low-frequency driving circuits. The maximum thrust force was obtained recently by Ref. [39] with a less speed compared to Ref. [25].

To achieve higher speed, the motor switching frequency and excitation voltage amplitude must be increased. A maximum operating frequency of 1000Hz has been achieved in Ref. [25] with a voltage of 124 V. The IM reported has the same operating voltage as [28], but exhibits lower speed due to a drop in operating frequency from 800 Hz to 30 Hz [37]. The maximum speed of the IM linear motor was obtained by Ref. [40] with reduced frequency and driving voltage compared to Ref. [25] as the former was loaded with maximum thrust of 0.6 N in order to achieve the high operating speed. It can be observed that frequency of operation plays a vital role in determining motor speed, however reported literature shows that piezoelectric inchworm motor could be operated up to a maximum frequency of 1000 Hz, thus limiting its speed potential. The majority of the IM configurations have designed a relatively high volume motor that uses three piezo actuators except in configurations [32,37,40] which have even more actuators. In this paper, the IM speed is increased by operating it at higher frequencies through proposed driver circuit along with a smaller motor volume and weight while keeping the number of piezo actuators unchanged.

Additionally, the Clamping Mechanism (CMs) of the proposed design locks the rotor when unpowered, unlike the configurations described in the literature [25,28,30,32,35,38,39] that require electrical signals for clamping. The design ensures two blocks on each of the CMs to apply a relatively high blocking force, making the structure self-locking at no power. External electrical excitation is required to de-clamp and unlock the stator from the rotor for a free stroke.

Thus, it is evident that piezo IM motors play an important role due to its simplistic construction and advantages of material properties. However, the reported developments center on low frequency drive and high motor volume. Consequently, the motors generate restricted motion which limits its usage for high speed industrial application.

Design and experimental analysis of a high force piezoelectric linear motor were proposed [41] where five PAs were used and excited at low frequency (1 Hz) resulting in speed of 2.25 μm/s. In the current paper, PA linear motor with similar performances is presented. The rotor is actuated by three PAs instead of five. Moreover, high frequency power supply (3 kHz) is developed and tested.

From a theoretical and mechanical perspective, the study demonstrates:

This study presents a design methodology for an inchworm motor based on finite element analysis (FEA) [42]. We focus on key design parameters, particularly the importance of a T-shaped rail to prevent derailment, which is crucial for ensuring stable motor operation. Additionally, we highlight the motor’s ability to maintain a locked state without energy consumption at rest, an important feature for energy management. The motor is designed to be compact, with high forces within a volume of only 44.72 cm^3. Furthermore, the study explores the selection of appropriate piezoelectric actuators and analyzes the clamping and unclamping mechanisms to ensure precise and efficient operation.

From a practical perspective, the study demonstrates:

The study demonstrates the feasibility of assembling the inchworm motor into a compact structure that includes all actuators and optimizes the arrangement of power supply wiring. One of the novel aspects of this research is the adjustment and balancing of the pre-stress force on both

Table 1
Performance of reported IMS

References	Driving frequency [Hz]	Speed [mm/s]	Driving voltage[V]	Maximum Thrust[N]	Number of Piezo Actuators	Volume[cm^3]
1999 [25]	1000	6	124	41.5	3	48
2003 [26]	15	0.0013	100	–	3	100
2006 [27]	–	20	–	10	3	–
2007 [28]	800	8.5	200	6	3	–
2011 [29]	600	3.60	100	–	3	–
2013 [30]	70	2	150	10	3	–
2016 [31]	8	0.005	120	43	3	280
2017 [32]	110	4	100	10	4	–
2018 [33]	180	26.74	10	–	3	44.55
2019 [34]	150	1.07	150	70	3	296
2020 [35]	50	0.72	120	3.28	3	202.6
2021 [36]	3.2	0.043	75	–	3	–
2021 [37]	30	0.028	200	4.9	2	169
2021 [38]	120	1.54	150	1.2	3	432
2022 [39]	250	0.043	120	546	3	112
2022 [40]	650	44.69	80	0.6	6	116.6

clamps, ensuring optimal performance. These practical advancements show that the proposed system is viable for real-world applications, especially in constrained industrial environments, such as in aeronautics (e.g., pilot seat actuation) and automotive industries (e.g., adjustable seating).

An one of the main challenges in powering inchworm motors is the overlap of supply voltages for the two clamping systems, which can reduce motor efficiency. In this study, we address this issue by introducing a phase shift between these voltages, optimizing their synchronization and reducing energy losses. Furthermore, by increasing the excitation frequency, we improve speed and overall performance. This research provides a comprehensive methodology for designing the power supply system for a three-actuator piezoelectric inchworm motor, ensuring precise control of the clamping and extension mechanisms while maintaining high energy efficiency.

The specific contributions of this work can be summarized as: i) Development of mechanical structure and prototype design of the IM, ii) Geometrical modelling of mechanical system and FEA analysis to investigate performance of CMs and Extending Mechanism (EM) of the IM, iii) Design and implementation of isolated mosfet based high switching frequency and high voltage driver circuit for long range, high speed linear translation application and its experimental verification, iv) Dynamic modelling of the IM and development of specially designed load end, electrical oscillator circuits, v) Experimental investigation towards performance evaluation of IM with varying the duty cycle, switching frequency and load.

Accordingly the research paper is organized into six sections.

The mechanical structure and design of control mechanism of the inchworm motor are discussed in Section II. FEA analysis of the IM is mechanism and prototype fabrication are presented in section III and IV. The mathematical modelling of the motor is derived in section V. Section VI presents the three phased isolated switching and boost driving mechanism while the experimental result analysis and verification of developed solution are presented in section VII, VIII respectively. Finally, conclusion is made in section IX.

2. Mechanical structure & IM mechanism

The proposed mechanical design mainly focuses on high clamping force requirement besides addressing the difficulties associated with the specific integration constraints. The main motive behind this work is to provide a clamping mechanism with full clamping abilities without the activation of the motor i.e self-locking at rest, which is often a required property cause self-locking feature at rest is a key aspect of our design, providing a significant advantage in energy efficiency by reducing power consumption during idle periods. By ensuring that the motor maintains a locked position without continuous activation, this feature prevents unnecessary energy usage. Previous reported inchworm motors often lacked such a self-locking mechanism, requiring continuous power to maintain clamping force even when not in motion. This approach resulted in higher energy consumption during rest, which is a limitation, particularly for applications where minimizing power usage is crucial. The challenge in our design was to incorporate a self-locking mechanism while maintaining a compact form factor 86 x 26 × 20 mm^3. Compact sizes typically restrict the space available for additional locking components. Our solution balances the need for high clamping force with the goal of achieving a small, energy-efficient design. This approach offers a more sustainable solution, especially in applications where energy conservation is paramount. The CM generates high blocking force with relatively compact size in terms of dimensions and performances detailed hereafter.

2.1. Proposed piezoelectric IM

The new design shown in Fig. 1 includes two CMs (green) and an extender (red) which are fitted with piezoelectric actuators (marked in blue). Screw and nut junction is used to connect the CMs and EMs while pre-tightening blocks and screws are used. Fixed part of the motor (stator) marked in grey is designed to act as a guide for the moving part as well as to lend a desired blocking force necessary for actuation.

The stator has a T-shape that prevents the rotor from derailing.

Screws (marked in orange) along with washer to clamp and spring are used in the design to necessitate a uniform blocking force on the inchworm motor's rotor, seen in Fig. 1. Stator of the motor is assumed to be completely rigid with no gap with the rotor. The rotor is blocked on stator through screws and nut. In order to deactivate the CMs, the PAs in the CMs are placed along Y-Axis.

Another interesting property of the designed motor is self-locking at rest. Powering up the PAs in the CMs, unlocks it while withdrawal of power, naturally blocks the stator. A very fine thread pitch was chosen which has a better technical resistance to loads and allows to have a solid connection but also to obtain a precise adjustment of the restressing force.

This force can be controlled by knowing the number of turns. Moreover, the contribution of the PAs is controlled since we have imposed the same pre-stressing force to balance the contribution of CMs by imposing the same level of applied voltage which can prevent the uneven force between the threads and the pitch gap of the motor.

The operating mechanism [43] of the IM comprises a cycle of six steps, as elaborated in Fig. 2.

3. Geometrical modeling & FEA analysis of the IM mechanism

To compute the performance of the IM for the CM and EM, 3D FEA

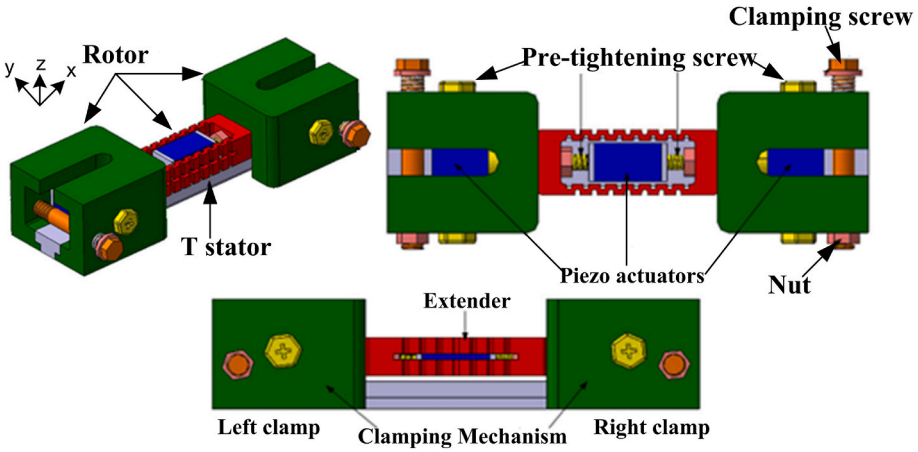

Fig. 1. Proposed piezo based IM design structure with self-locking at rest.

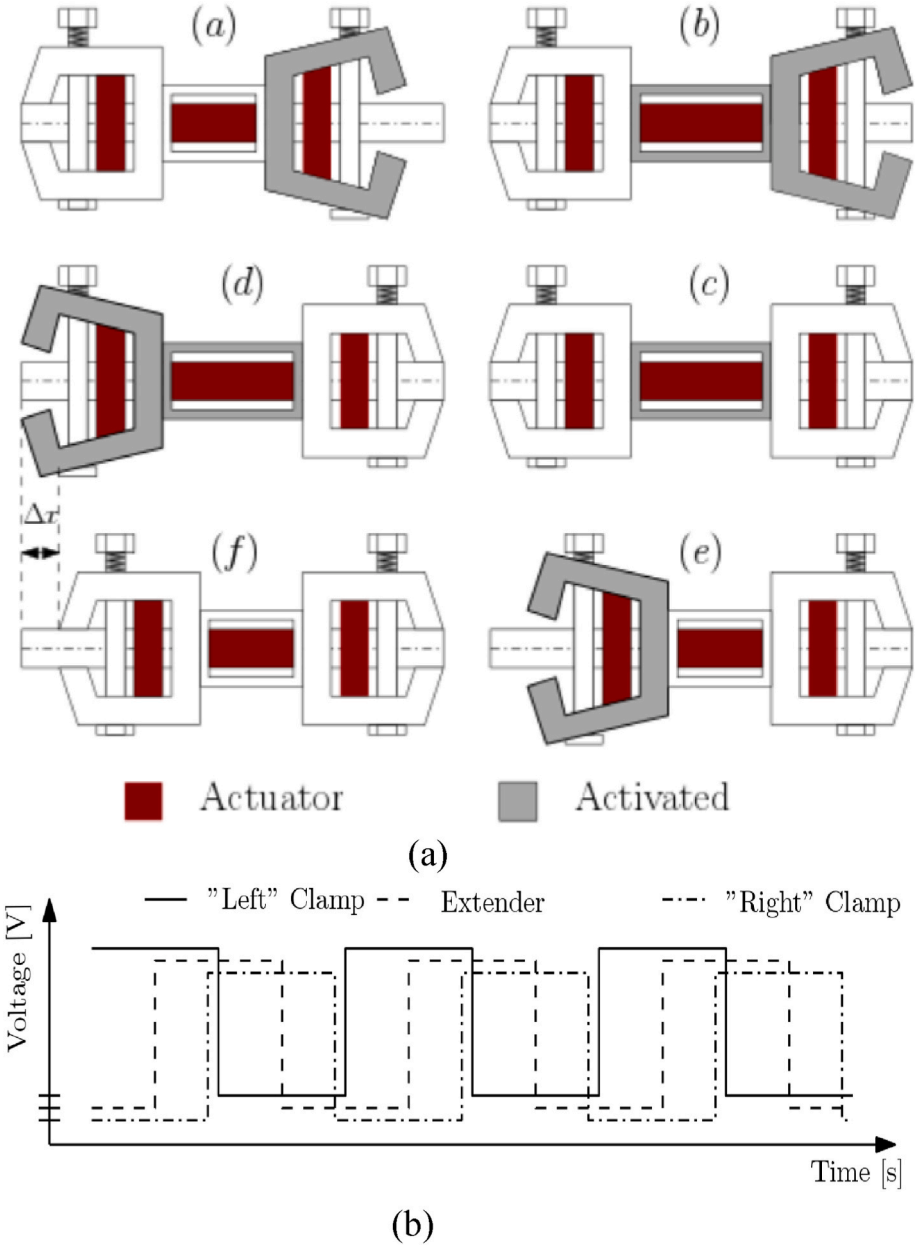

Fig. 2. a) IM operating mechanism comprising six steps. b) Motion generation voltage curve for IM during three cycles.

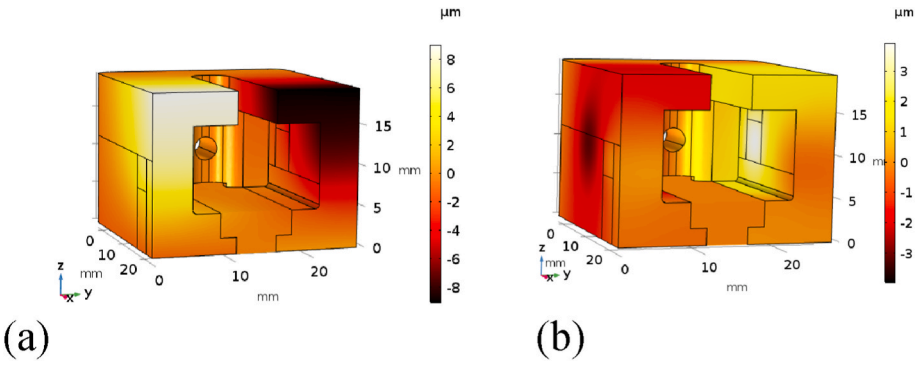

Fig. 3. Clamp displacement distribution along Y-axis a) In the closing mode b) In the opening mode.

has been conducted using COMSOL Multiphysics® software.

3.1. Clamping mechanisms

Fig. 2 shows that the slider is clamped when the rotor is off. The dimensions shown in Fig. 3 were chosen to obtain a high holding force. Since the displacement of the chosen PA is limited, it was placed as far as possible from the clamping region (the displacement is amplified).

Clamping mechanism has been designed such way to minimize any shear forces acting directly on the piezoelectric stack. The design ensures that the piezoelectric stack is subjected primarily to axial forces, which are aligned with its inherent motion. Any lateral or shear forces are minimized by carefully optimizing the geometry of the clamp. Additionally, the clamp unit includes features such pre-tightening blocks between the piezoelectric stack and the clamp surfaces (element with grey color on the actuators), which help to distribute the forces more evenly and further reduce the risk of shear damage.

Several materials were modelled to optimize the stiffness regarding dimensions. The selected material is steel (for high friction force rotor/stator) with a density of 7860 kg/m^3, elastic modulus of 200 GPa, and poisson ratio of 0.266. In this work, steel over aluminum has been chosen for the motor's design based on several key considerations. Steel provides significantly higher stiffness compared to aluminum, which is essential for maintaining performance consistency given the characteristics of the Noliac Piezoactuators utilized in the motor. If aluminum was used, longer piezoelectric actuators would be required to achieve similar stiffness, which would increase cost, weight, and motor volume, ultimately compromising the design's compactness and efficiency. Furthermore, while aluminum has a higher static friction coefficient than steel, the dynamic friction coefficient of steel is lower. This lower dynamic friction is beneficial for the motor's sliding motion, enabling smoother operation compared to aluminum.

3.1.1. Clamp closure

By the clamping screw, a total contact force(along Y-axis) of 1250N is obtained under applied screw force of 730 N on both sides. The corresponding clamp displacement distribution along Y-axis in the closing mode is presented in Fig. 3(a).

3.1.2. Clamp aperture

Modeling results indicate that when PA applies a 1600 N force over the clamp, the reaction force on the slider from the clamp is 0. Fig. 3(b) displays the displacement trajectory on applying a force of 1600 N to the PA along Y-axis. At the position of the PA, a displacement of 12 μm (6 × 2 μm) is induced. Hence, a PA with stiffness of 133 Nμm^{-1} is required.

3.1.3. Clamp closure and aperture in the contact region

The transition between clamp closure and clamp aperture is analyzed. The Von-Mises stress when the clamp is locked and unlocked through the T-rail is shown in Fig. 4. (a) and Fig. 4(b) respectively. The absence of stress along the T-rail (contact region) when the clamp is open (Fig. 4 (b)) is the evidence of a zero contact force.

From these two tests, the contact region between stator and rotor was examined. As can be seen in Fig. 5, when the clamp is closed, the displacement has the same pattern in both clamp and T-rail, because the force applied by the clamp is transmitted to the rail through the contact region. Near the clamping screw (position 17 mm), the rail displacement is 1 μm due to the applied force. However, when the clamp is open (a PA force is applied in addition to that of the screw), the distance between rotor and stator increases creating a gap of 2 μm in the region of the PA (No contact between stator and rotor).

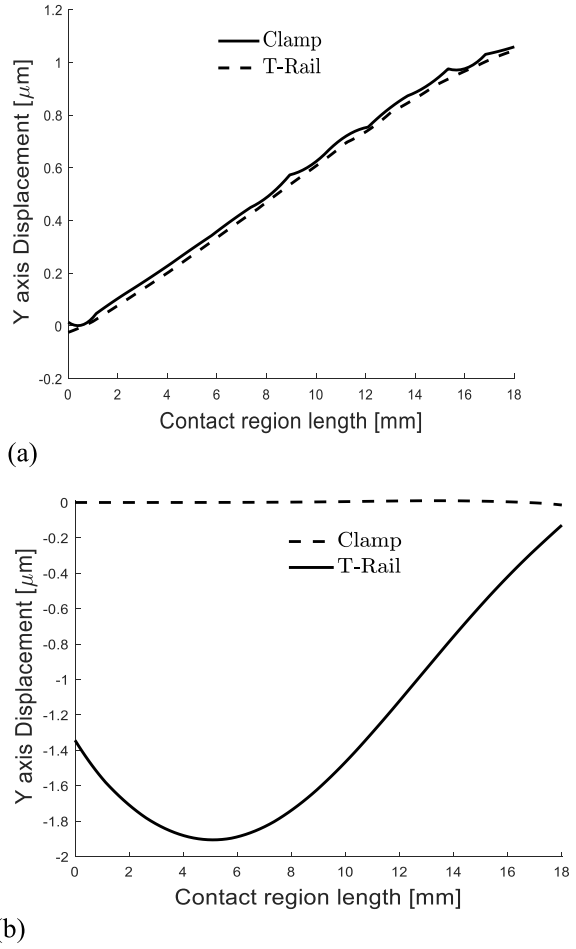

Fig. 5. Displacement at clamp closing (a) and opening (b) in the contact region.

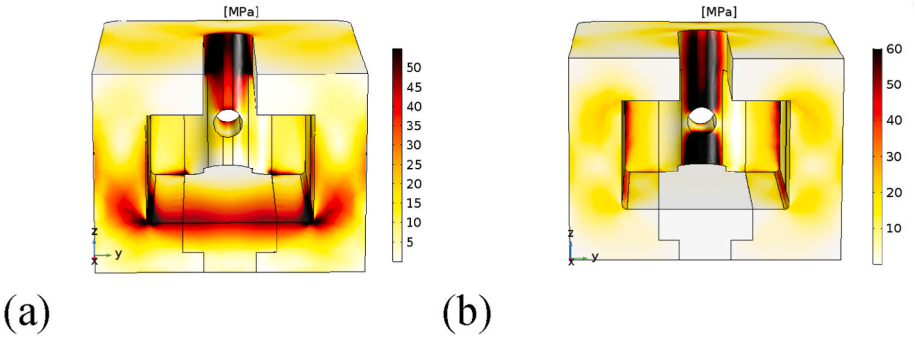

Fig. 4. Von-Mises stress, (a) Clamp closure (b) Clamp aperture.

3.2. Extending mechanisms

PA is typically used in a metal case to improve reliability, as there is no direct linear contact between the two clamping mechanisms.

In the clamp system, the clamp itself creates the pre-tightening force while, in the EM, we have to design a metal casing which also safeguards the actuators from external hazards and force impacts. The design is centered around the elasticity property of the extending mechanism with its length and breadth dimensions being limited to that of the clamps. The extender, thus, operates as a spring when the PAs are powered on.

3.3. Extending and retracting mode

Modeling results indicates that a displacement of 13 μm is obtained when a 500 N force is applied to the elastic case, Fig. 6(a). Upon withdrawal of power from the extender, it retracts which is ensured by the fact that the Von-Mises stress is less than the yield stress stainless steel. It was verified through calculation of Von-Mises stress that the elastic limit was not reached, as seen in Fig. 6(b). Selection of proper piezo actuator in terms of required force at output, displacement range required, and dimensional restrictions, is hence possible with a knowledge of the inchworm motor stiffness.

4. IM prototype manufacturing and assembly

4.1. PAs characteristic

An intersection of the force displacement graph with the motor structure stiffness is required as the force generated by the PA is linked with reduced elongation. In the experiments, multi-layer NOLIAC piezoelectric stack actuators [44] have been used –NAC 2022H14 [45] and NAC 2021H16 [46] for clamps and extender respectively. Specification of PZT stack actuators are given in Table II. Voltage vs displacement characteristics of the piezo-actuators are measured at off-load condition, represents a linear relationship, Fig. 7.

4.2. Prototype assembly

A prototype with dimensions 86 × 26 × 20 mm^3 and a weight of 200 g was manufactured. The three individual parts (clamp 1, extender, clamp 2) of the inchworm motor are assembled with the corresponding PA in the clamp and in extender structure as shown in Fig. 8. Traveling range of the proposed inchworm motor is not inherently limited by the piezoelectric actuators themselves but is determined by the design of the system, particularly the length of the guiding structure and the stroke length of the actuators. In our experimental setup, motor achieves a range of approximately 200 mm. This range can be extended by modifying the mechanical design or integrating additional stages, as long as the clamping and driving mechanisms maintain stability and precision.

Table 2
Specification of piezoelectric stack used in the IM.

Type	Dimensions [mm^3]	Free stroke [μm]	Blocking force [N]	Capacitance [μF]
CM: NAC2022-H14	10 × 10 × 14	19.8	4200	2.38
EM: NAC2021-H16	7 × 7 × 16	23.1	2060	1.39

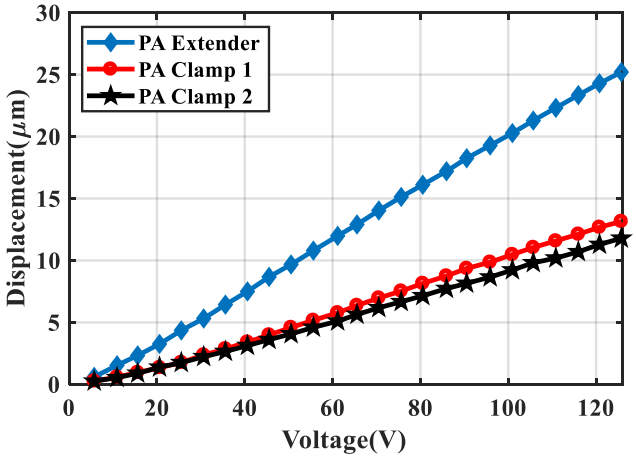

Fig. 7. Forward stroke displacement of free PAs versus applied DC voltage.

4.3. Pre-stress force measurement of PAs using force sensor

The PAs used in the development of the IM need to be calibrated for accurate system response. Pre-stress forces have been applied by the Compression Digital Hand Tester (CHDT) to the PA and the corresponding analog voltage signals have been observed in DSO, as measured by the force sensor, seen in Fig. 9 (a). Pre-stress force is increased from 80 N to 200 N and corresponding change of voltage are increased from δ_5 to δ_1 ($\delta_1 > \delta_2 > \delta_3 > \delta_4 > \delta_5$). It is seen that the maximum pre stress force 200 N can be measured at change of voltage δ_1. The force vs voltage plot of the experimental pre-stress measurement data (Fig. 9 (b)) suggests the dependency of voltage on force of the PAs is linear.

The values of prestress/preload applied to the three piezoelectric actuators for the IM are approximately 50 N. This force was applied in a balanced manner, based on the number of turns of the adjustment screw. For further details regarding the method used to impose this force, refer to [41].

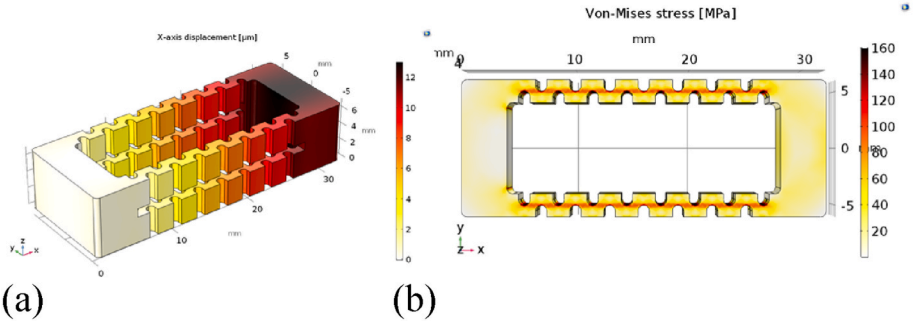

Fig. 6. a) Extender displacement distribution in the extending mode along X-axis (3D view) b) Extender retracting mode along X-axis(3D).

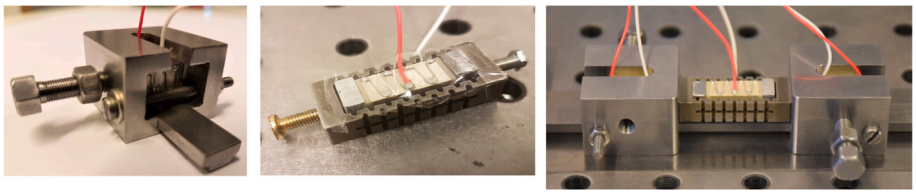

Fig. 8. Inchworm Motor (IM) prototype, (a) Clamping Mechanism (CM) with PA, (b) Extender Mechanism (EM) and (C) fabrication of constituent parts.

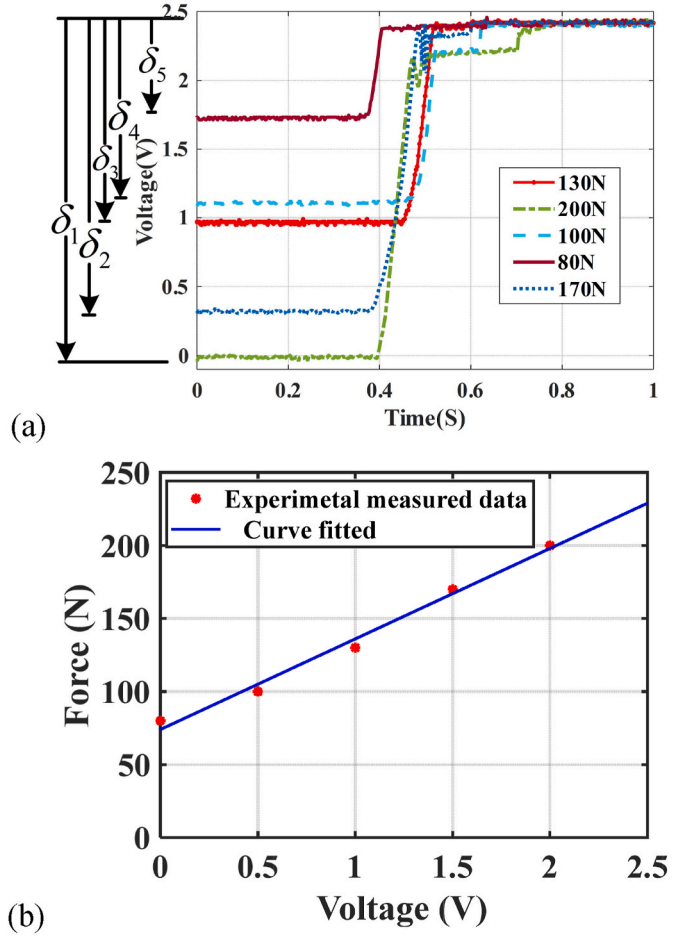

Fig. 9. a) Prestressing force measurement plot of PA for IM b) force vs voltage relationship of PA with linear curve fitting.

5. Mathematical modeling of the inchworm motor

In this section, dynamic modelling of piezo-based IM is developed in MATLAB Simulink platform to ensure that positive driving pulses traverse across the piezo-actuators of the motor. The normal applied force is directly proportional to the applied voltage of the motor. Resultant linear displacement by the motor is achieved due to movement of extender fitted between the two clamps and the rotor.

The frictional force can be defined as which are combination of coulomb and stiction adopted for modelling friction between the clamping chambers and the guide walls [47] expressed as

$$F_{fr}(V,\dot{x}) = \begin{cases} -aVsgn(\dot{x}), |\dot{x}| \geq v_0 \\ -F_0 sat\left(\frac{aV}{F_0}\right), |\dot{x}| < v_0 \end{cases},$$

Frictional force between guide wall and clamping chamber is represented as equation (5), where, $\dot{x}_{c1}$ and $\dot{x}_{c2}$ are the velocity of left and right clamps with V_{c1}, V_{c2} and V_e being the applied voltage on the two clamps and extender. A small speed v_0 ($v_0 > 0$) is defined to represent the situation at which the body can be considered stationary (e.g. $\dot{x}_{c1}, \dot{x}_{c2} < v_0$). The co efficient 'a' of equation (5) is constant which is proportional to the friction co-efficient 'μ' and can be calculated by piezoceramic one dimensional equation [48]

The sign and saturation function can be defined as $sgn(x) = \begin{cases} 1, & x > 0 \\ 0, & x = 0 \\ -1 & x < 0 \end{cases}$, $sat(x) = \begin{cases} 1, & x > 1 \\ 0, & -1 \leq x \leq 1 \\ -1 & x < -1 \end{cases}$

F_0 represents either F_{0C1} and F_{0C2} which are the sum of the forces acting on clamp 1 and clamp 2 of the inchworm motor respectively. They are defined as

$$F_{OC1}(X,\dot{X},V_e) = -F_P(V_e) + k_l(x_e - x_{c1}) + C_{c1}(\dot{x}_e - \dot{x}_{c1}) \quad (1)$$

$$F_{OC2}(X,\dot{X},V_e) = -F_P(V_e) + k_{c2}(x_e - x_{c2}) + C_{c2}(\dot{x}_e - \dot{x}_{c2}) \quad (2)$$

Where, x represents position vector represented as.

$$x = \begin{Bmatrix} x_{c1} \\ x_e \\ x_{c2} \end{Bmatrix}^T$$ x_{c1} = displacement of clamp1, x_e = displacement of the middle actuator or extender, x_{c2} = displacement of the clamp 2 of the motor, V_e = voltage applied to the extender piezo stack, F_P () represents as a pushing force exerted by the piezoelectric stack actuator on the mechanical structure.

The dynamic model of proposed piezoelectric IM represented in Fig. 10 has been mathematically modelled as

$$M\ddot{X} + C\dot{X} + KX = F_{fr} + F_P \quad (3)$$

where, F_{fr} represents the frictional force and longitudinal piezo stacks exert a pushing force on the motor frame of the motor which is indicated by F_P.The system can be designed in non-linear state space form as

$$\dot{x} = [A]x + g(u,x), y = [C]x \quad (4)$$

where, [A] and [C] are input, output matrix of the system, 'y' is displacement of the middle actuator (extender) and 'x', 'u' are the system state, input vector, accordingly and defining them as follows:

$$x = \{x_{c1} \quad x_e \quad x_{c2} \quad \dot{x}_{c1} \quad \dot{x}_e \quad \dot{x}_{c2}\}^T u = \{V_{C1} \quad V_E \quad V_{C2}\}^T$$

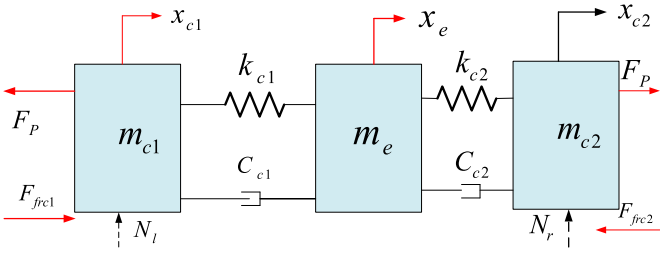

Fig. 10. Dynamic model of the Inchworm motor.

$$g(u,x)=\begin{Bmatrix}0\\0\\0\\F_{frc1}(V_{c1},\dot{x}_{c1})-V_ed\\0\\F_{frc2}(V_{c2},\dot{x}_{c2})+V_ed\end{Bmatrix}^T, C=\{010000\}$$

A single PA can be modelled as second order spring mass damper system [49]. As IM is designed using three piezoelectric stack actuators, the overall system can be represented as a second order mass spring damper system with the two clamps and one extender of the motor being represented through equations (6)–(8) respectively.

where, C_{c1} = damping coefficient of clamp 1, C_{c2} = damping coefficient of clamp 2, k_{c1} = stiffness of the clamp 1, k_{c2} = stiffness of the clamp 2, K = stiffness of longitudinal piezo stacks, m_{c1} = mass of the clamp 1, m_e = mass of the extender, m_{c2} = mass of the clamp 2. Dynamic equations (6)–(8) are used to design the proposed inchworm motor.

6. System description

The block diagram of proposed electrical driving system is shown in Fig. 11 where a high switching isolated driver circuit for piezoelectric actuator based IM is developed which includes three step-up converters and three mosfet based switching circuits for the two clamps and one extender. Three isolated 24 V battery sources are used as an input power supply to operate the whole system because motor has three phases and each of phase should be isolated to each other. Three DC-DC step-up high wattage non isolated converters have been developed to step up the voltage from 24 V to 120 V DC.

The integrated controller of the step up converter can control the magnitude of the driving voltage. Isolated mosfet based switching circuits (IMSC) generates three isolated phase shifted synchronized pulse for two clamps (80 V magnitude) and one extender (90 V magnitude) for the IM besides isolating the microcontroller control pulses from the driver unit.

$$F_{frc1}(V_{c1},\dot{x}_{c1})=\begin{cases}-aV_{c1}\mathrm{sgn}(\dot{x}_{c1}), |\dot{x}_{c1}|\geq v_0\\ -F_0 sat\left(\frac{aV_{c1}}{F_0}\right), |\dot{x}_{c1}|<v_0\end{cases}, F_{frc2}(V_{c2},\dot{x}_{c2})=\begin{cases}-aV_{c2}\mathrm{sgn}(\dot{x}_{c2}), |\dot{x}_{c2}|\geq v_0\\ -F_0 sat\left(\frac{aV_{c2}}{F_0}\right), |\dot{x}_{c2}|<v_0\end{cases} \quad (5)$$

Dynamic equation for clamp 1 system is

$$\ddot{x}_{c1}=-\frac{C_{c1}}{m_{c1}}\dot{x}_{c1}+\frac{C_{c1}}{m_{c1}}\dot{x}_e-\frac{k_{c1}}{m_{c1}}x_{c1}+\frac{k_{c1}}{m_{c1}}x_e-\frac{K}{m_{c1}}x_{c1}+\frac{K}{m_{c1}}x_{c2}-\frac{V_ed}{m_{c1}}+\frac{F_{frc1}(V_{c1},\dot{x}_{c1})}{m_{c1}} \quad (6)$$

Dynamic equation for extender system is

$$\ddot{x}_e=-\left(\frac{C_{c1}}{m_e}+\frac{C_{c2}}{m_e}\right)\dot{x}_e+\frac{C_{c1}}{m_e}\dot{x}_{c1}+\frac{C_{c2}}{m_e}\dot{x}_{c2}+\frac{k_{c1}}{m_e}x_{c1}+\frac{k_{c2}}{m_e}x_{c2}-\left(\frac{k_{c2}}{m_e}+\frac{k_{c1}}{m_e}\right)x_e \quad (7)$$

Dynamic equation for clamp 2 system is

$$\ddot{x}_{c2}=-\frac{C_{c2}}{m_{c2}}\dot{x}_{c2}+\frac{C_{c2}}{m_{c2}}\dot{x}_e-\left(\frac{K}{m_{c2}}+\frac{k_{c2}}{m_{c2}}\right)x_{c2}+\frac{K}{m_{c2}}x_{c1}+\frac{k_{c2}}{m_{c2}}x_e+\frac{V_ed}{m_{c2}}+\frac{F_{frc2}(V_{c2},\dot{x}_{c2})}{m_{c2}} \quad (8)$$

6.1. Design of equivalent oscillator circuit at load end to actuate capacitive piezo element at high frequency

An equivalent oscillator circuit is designed across each PA of the IM to operate the motor around resonant frequency (derived in eqn (9)) to achieve maximum output power and efficiency. A designed inductor 271 μH for each clamp and 318 μH for the extender are connected in parallel

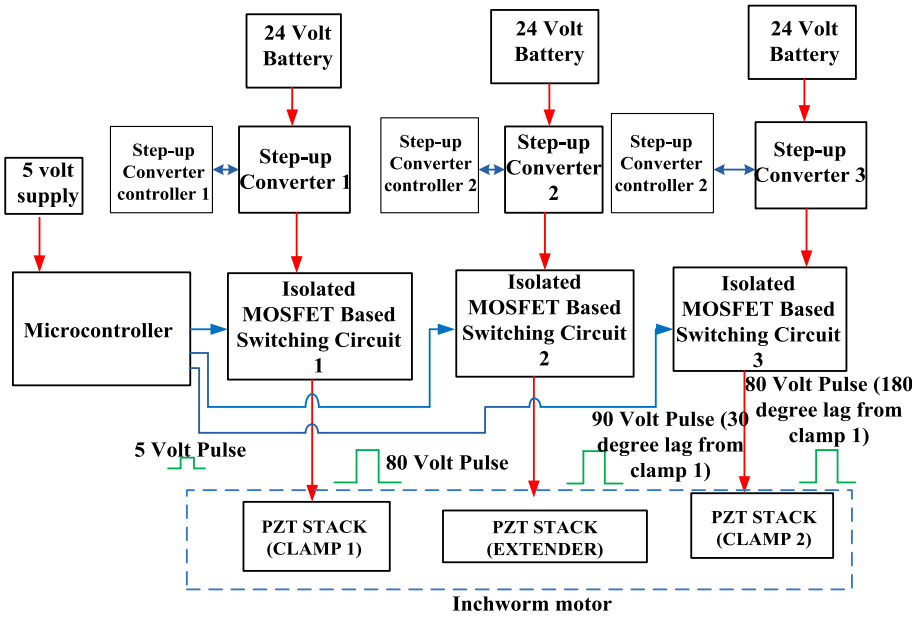

Fig. 11. Block diagram of the proposed electrical driving system of IM.

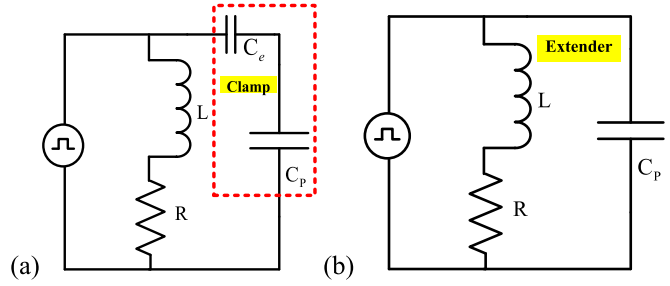

Fig. 12. Equivalent oscillator circuit diagram for operation of the IM connected at load end of each stack actuator a) clamp b) extender.

across the piezo-actuator to make the overall circuit resistive in nature at resonance and eliminate reactive power. An external capacitor (C_e) is connected in series to the capacitive clamp PA ($C_P = 2.38\ \mu F$) to reduce the equivalent capacitance value as well as to increase the operating frequency of the clamp circuit as shown in Fig. 12 (a).

$$f = \frac{1}{2\pi}\sqrt{\left[\frac{1}{LC_P} - \frac{R^2}{L^2}\right]} \tag{9}$$

The inductor value of the circuit is set as per

$$L = \frac{1 \pm \sqrt{(1 - 4\omega^2 {C_P}^2 R^2)}}{2\omega^2 C_P} \tag{10}$$

Accordingly, the frequency range should be $4\omega^2 C^2 R^2 < 1$

$$\text{Therefore, } f < \frac{1}{4\pi C_P R} \tag{11}$$

With an equivalent capacitance of the clamp circuit as 1.19 μF and assuming the resistance to be 15 Ω, the operating frequency range is found to be f < 4.46 kHz for NAC 2022H14 two PZT stacks and f < 3.818 kHz for NAC2021H16 PZT stack for the extender.

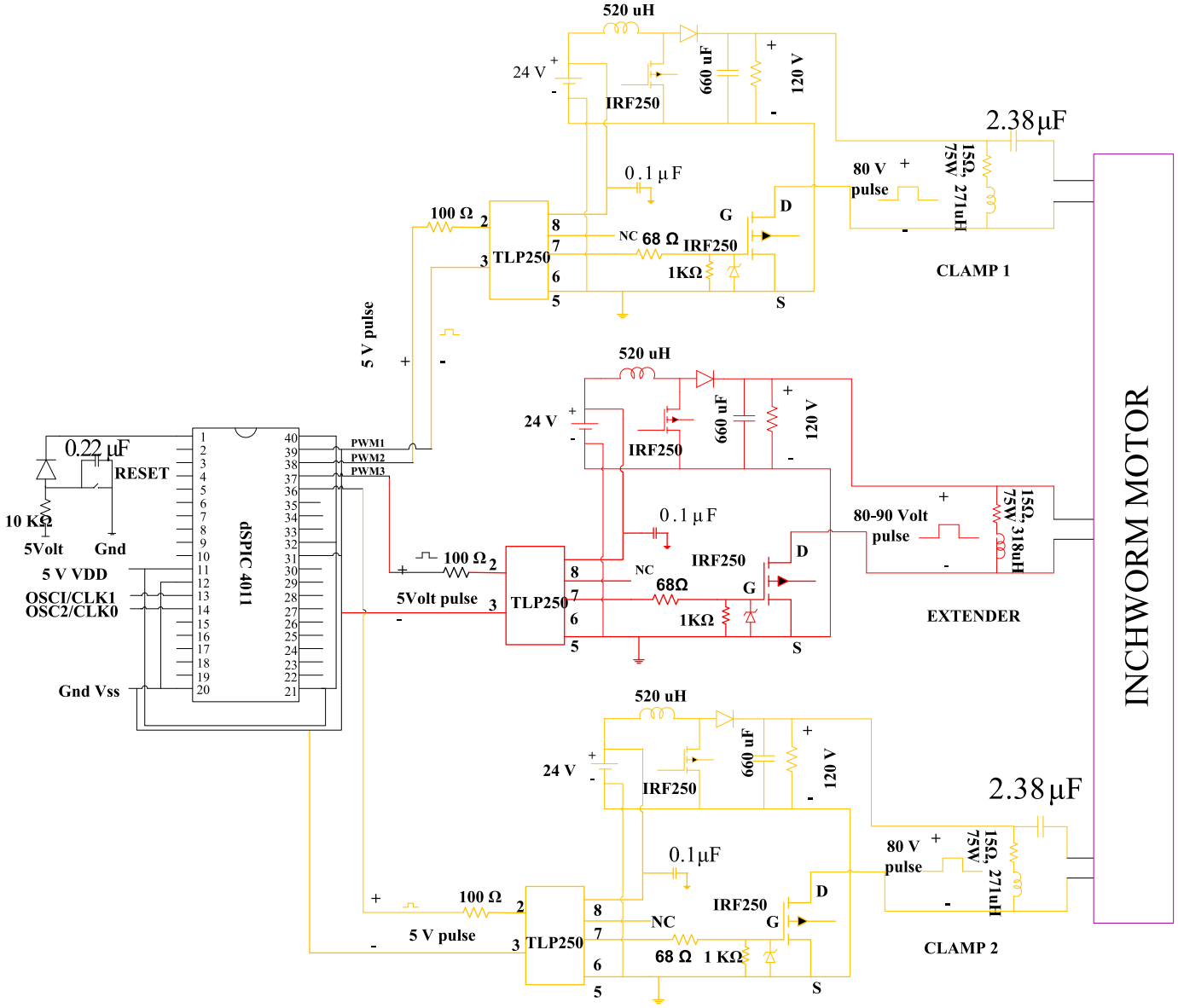

Fig. 13. Circuit diagram of driver unit for actuation of IM.

6.2. Circuit diagram of high switching driving unit

Digital micro-controller dsPIC30F4011 is used to generate three phase synchronized 5 V magnitude control pulses to actuate the inchworm motor in-line with the operating principle shown in Fig. 13. The three control pulses have been isolated from driver circuit through opto-coupler based gate driver. The two clamps are applied with PWM pulses with 180° phase shift while extender is subjected to a 30° phase shift. The switching frequency varies between 50 and 3000 Hz, operating at duty cycle of 20 % and 30 %. During the operation of each IMSC, 80–90 V magnitude positive square pulse is generated between the positive terminal of the output of each step up converter and drain terminal of the mosfet, to drive the IM.

7. Experimental result and analysis

The experimental test bench set up of the proposed system is illustrated in Fig. 14. An IMSC inchworm motor driver circuit has been developed to generate appropriate driving signal from respective control pulses to actuate the motor. An opto NCDT laser displacement sensor ILD2300 (Resolution of 0.8 μm at 20 kHz frequency) is interfaced to the motor for measuring the displacement at higher frequencies. The laser displacement sensor is connected to the C-Box and ILD2300 sensor tool software is accessed through the ethernet port of the C-box. As discussed in section IV, the experimental setup considers blocking force as 5 N, and loads are attached to the motor's rotor through a pulley arrangement system for testing. In this experimental work, the clamping force and maximum driving force are significantly different from the theoretical analysis (section III) and maximum performance of the motor has not been tested due to limitation of switching frequency and applied driving voltage level of the driving circuit.

7.1. IM step displacement curve at lower operating frequency without loading effect

The step displacement of the inchworm motor (11 cycles) and zoom viewed of two cycles are shown in Fig. 15, wherein Ch_3 voltage were used to operate the actuators in left clamping mechanisms, resulting in a axial displacement which releases the clamp from stator. Consequently, Ch_2 voltage is used to excite the extender, and the corresponding displacement is recorded. The left clamping mechanism gets released and right clamping mechanism (Ch_1) gets activated during the later half of Ch_3. Retraction of the left clamp and its return to previous dimension can be related to reduce observed displacement in DSO. As the displacement is recorded on the left CM which is closed, a fixed displacement is obtained in this interval. The step value of one loop (6 steps), according to Fig. 2, correspond to 2.5 μm, as indicated at time value of 4s in Fig. 15.

Back movements of IM have been seen in lower frequency operation during one cycle which it is challenging to eliminate these backward movements entirely, they can be minimized by optimizing the synchronization of the clamping and driving phases. In the experiment, as shown in the figure below, the two clamps of the motor are excited with a 180-degree phase shift (Ch_1 and Ch_3). This leads to the intersection of the two signals, meaning that at a given instant (for example, at 2s), both clamps are energized. In this state, both clamps are practically open, which limits the load and the test conditions. Specifically, the clamping force should always be higher than the driving force, and Ch_3 should begin only after the voltage of Ch_1 returns to 0, as reported in Fig. 16. Furthermore, at time t = 3s, this relates to the high driving force, which should be reduced to minimize backward movements.

7.2. IM tested at 1 kHz switching frequency without loading effect

The IM has been tested at high switching frequency of 1 kHz with 30 % on-time phase synchronized driving pulses (Fig. 16), the corresponding displacement and speed have been measured by laser displacement sensor to be 3.76 mm and 5.88 mm/s respectively. Displacement is observed to increase linearly when motor moves in forward direction as shown in Fig. 17(a) and (b).

7.3. Performance characteristics of IM with varying duty cycle and switching frequency at No load

Performance of the IM was tested at different operating frequencies and duty cycles. Duty cycle is the ratio of linear actuators running vs resting time typically varies range of 10–70 % and mostly depending on load. Increasing the speed and load on PA can lead to overheating, which reduces the actuator's life expectancy. Therefore, to increase load capacity and speed, driving pulse duty cycle has been decreased.

Displacement of the IM has been measured experimentally by laser displacement sensor. The driving frequency of the motor is linearly varied up to 1500 Hz at 30 % duty cycle, resulting a speed of 13.88 mm/s, as shown in Fig. 18. (a) The motor is further operated from 1750 Hz to 3000 Hz at 20 % duty cycle and in this case the speed variation of the inchworm motor is seen to be better than the operation at 30 % duty. Maximum speed of 60.15 mm/s is achieved at 3 kHz frequency with 20 % duty cycle. Frequencies of the driving signal of the inchworm motor are varied from 1 kHz to 3 kHz at 20 % duty to realize the desired motion, Fig. 18 (b). It is seen that when the motor is operated at higher frequency, it takes lesser time to bring about the desired motion compared to lower frequency operation. Fig. 18(b) shows a slight fluctuation which may be caused by vibration of the motor due to its high switching frequency or rough contact between the stator and rotor.

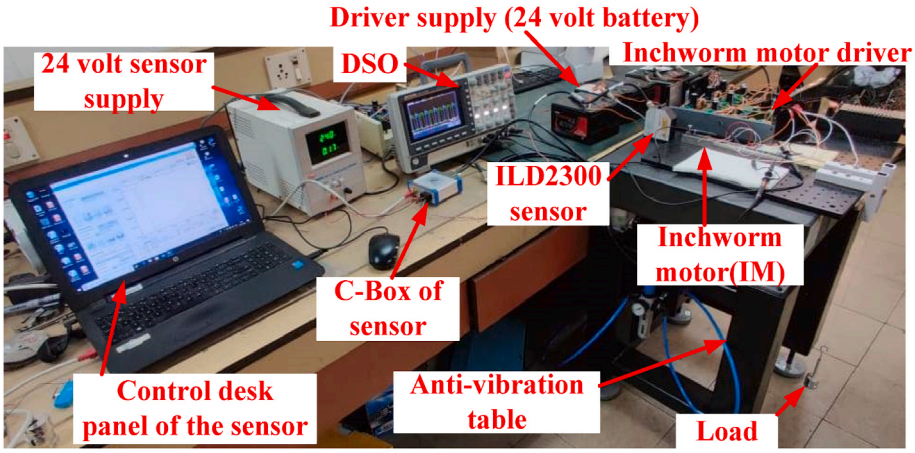

Fig. 14. Experimental test bench set-up for the proposed system.

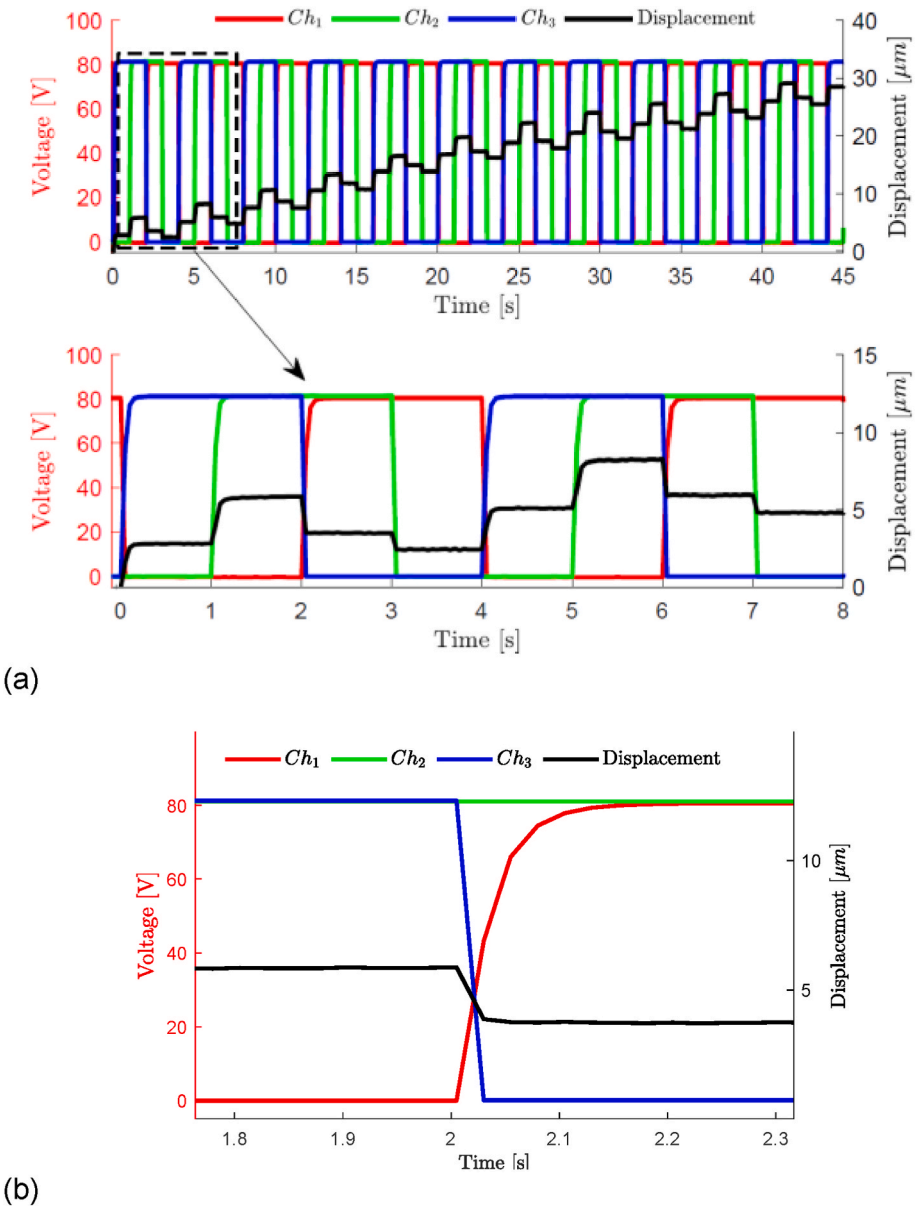

Fig. 15. a) Step displacement curve of 11 cycles at 0.25 Hz frequency b) Zoomed view plot of Fig. 15 a) (time span t = 2.3 s).

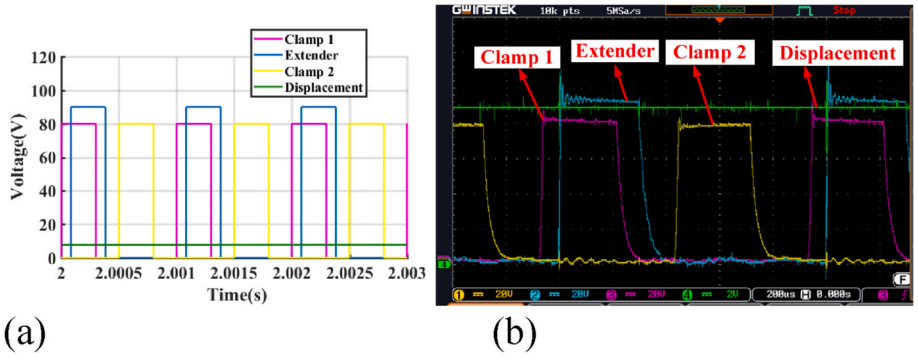

Fig. 16. a) Simulated from model: displacement (in term of voltage) waveform shown in green; positive driving voltage (1 kHz) waveform for forward linear motion of the IM: violet and yellow are two clamp signals (80 V), blue is extender signal (90 V) b) experimental. (For interpretation of the references to color in this figure legend, the reader is referred to the Web version of this article.)

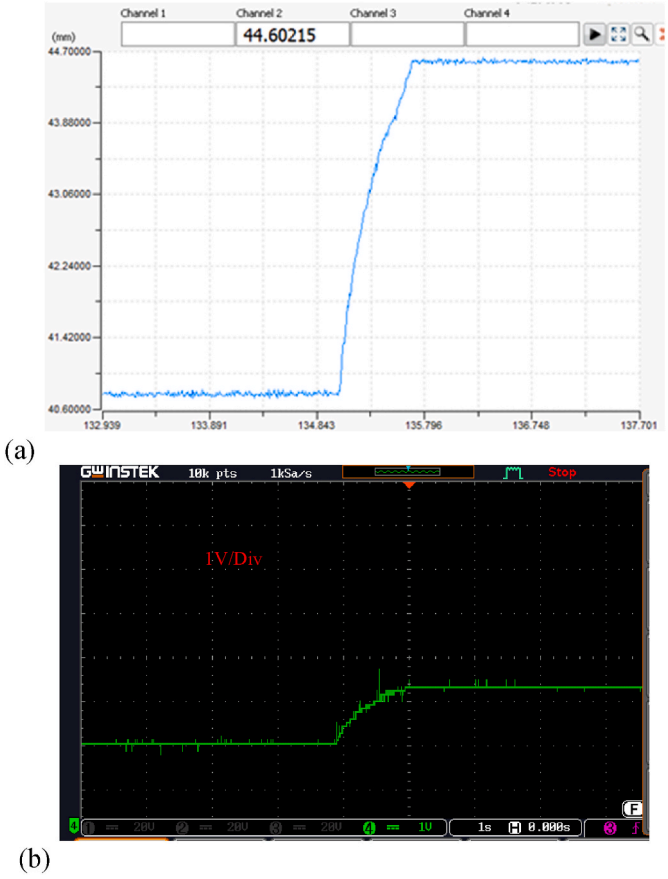

Fig. 17. a) Displacement plot of forward direction linear motion of the proposed IM b) corresponding linear variation of displacement in term of voltage observed in DSO.

7.4. Displacement and speed characteristics with variation of load

The motor has been experimented under different loading effect using 1.5 kHz 30 % duty cycle control pulse. Displacement and speed linearly decreases due to increase in load as reflected in Fig. 19 (a). Speed of the motor decreases from 0.87 mm/s to 0.45 mm/s with an increase of load from 2 N to 4 N. Displacement and speed characteristics of inchworm motor are shown in Fig. 19 (b) when operated at 3 kHz frequency and 20 % duty ratio.

At load of 4.41 N, the speed of the motor is measured to be 0.64 mm/s. Thus, the loading capability is seen to improve if the motor is operated at higher switching frequency and lower duty ratio. The inchworm motor is then operated with different loading capacities at different frequencies against a 2 N load attached the IM through a cable and pulley setup as seen in Fig. 20 (a). Motor is operated at 80–90 V and tested at different frequencies mentioned in fig. The speed vs frequency bar diagram of the IM is shown in Fig. 20 (b), where the motor driven at 3 kHz can pull a load of 2 N at a speed of 2.89 mm/s. The motor speed increases with increasing frequency regardless of whether it is loaded or not.

7.5. Efficiency calculation

Measurement was done by calculating the mechanical work during given period of time, corresponding to its power consumed, calculated by measuring the voltage and current of each channel as shown in Table III. Efficiency (electrical input power to mechanical output power) of IM is calculated 29 % (operating voltage 80–90 V and frequency- 3 kHz) which is better than 17 % reported for electrostatic inchworm motor operated at 110 V and 600 Hz frequency [29].

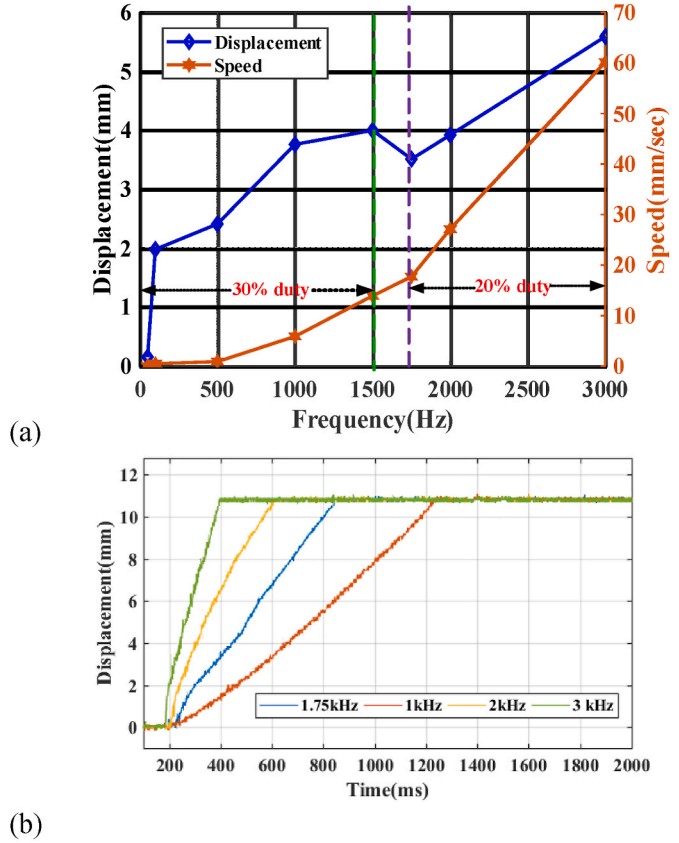

Fig. 18. a) Experimental displacement and speed measurement plot of IM by varying operating frequency and duty cycle b) Experimental operating characteristics of IM at different frequency.

8. Verification of developed solution

Experimental multi-parameter comparison of the developed IM was carried out with similar works reported earlier at low operating frequency [29,40,50–57] as shown in Table IV. The present design can actuate at a wide range of operating frequency, up to 3 kHz which is sixty times of IM mentioned in Ref. [53]. Consequently our design attains a maximum speed of 60 mm/s which 344 times of recent reported work [57] makes it a promising candidate for high speed, millimeter range longitudinal displacement.

9. Conclusion

In this research, piezo-based linear inchworm motor is proposed, designed and tested which achieves millimeter range displacement with better efficiency. The paper focuses on the modeling and FEA analysis of inchworm along with high clamping force requirement with specific integration constraints. Measurement of the pre-stress was carried out to improve the mechanical output ability. The proposed IM prototype could simultaneously achieve high frequency, high voltage operation by mosfet-based control and electrical capacitance balancing circuitry designed across piezo-actuators. Performance characteristics were then experimentally evaluated with different operating parameters such as frequency, duty cycle and loading effect. The motor can be operated at a maximum frequency of 3 kHz with 20 % duty cycle and achieves maximum no-load speed of 60 mm/s.

Experimental measurements of the prototype motor reveal a stroke length of 0.82 μm at 20 V, slightly lower than the nominal displacement of 1.67 μm for the individual piezoelectric actuator stacks. This variation

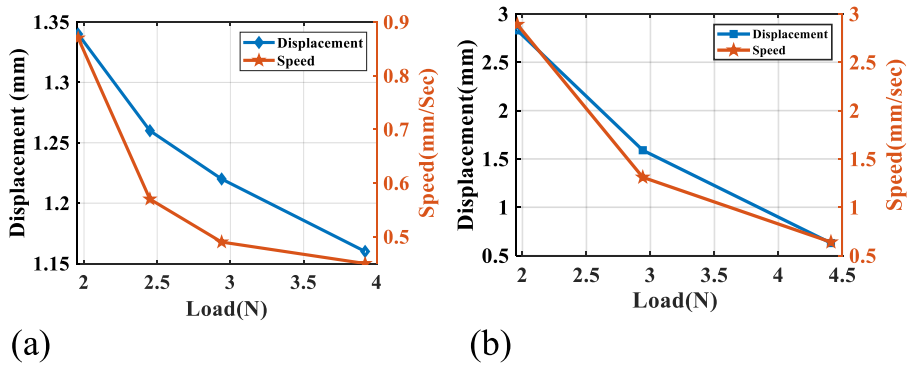

Fig. 19. a) Experimental displacement and speed characteristics of IM due to load variation for 1.5 kHz 30 % duty b) Experimental displacement and speed characteristics of IM due to load variation for 3 kHz 20 % duty.

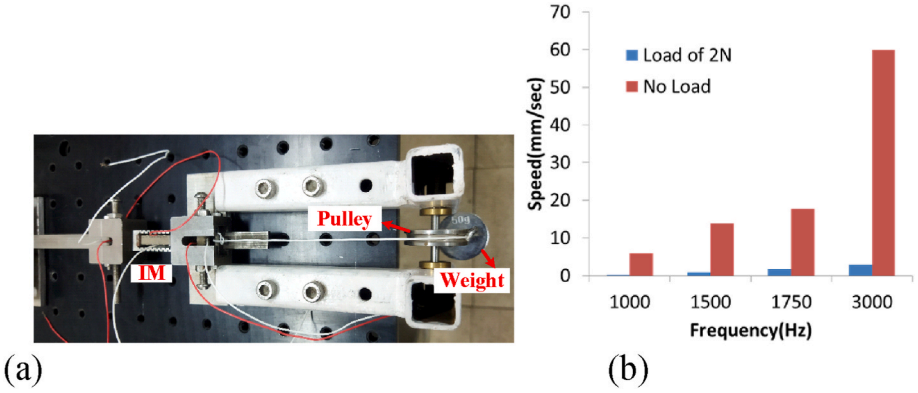

Fig. 20. Impact on speed of the motor with variation of frequency with and without load.

Table 3
Efficiency calculation of electrical driver and IM.

Measurement of efficiency	Output power of electrical driver		Input power of electrical driver		Efficiency (%)
	CM1 [W]	EM [W]	CM2 [W]	EM [W]	
Electrical driver efficiency while the IM is operated at no load	44.73	7.98	107	16.2	42
Mechanical efficiency of IM with driving load of 0.98N	31.7	4.34	104	17.21	29

is attributed to internal mechanical losses and assembly tolerances. When operated at higher voltages in the range of 80–90 V, the motor achieves a step length of 6 μm, coupled with a blocking force of 5 N under no-load conditions.

The repeatability of the motor's performance can be observed in the displacement curves provided in Fig. 15, where all cycles demonstrate consistent behavior. This repeatability is ensured by precise stroke control, which is governed by the applied voltage and the excitation frequency (number of cycles). The results highlight the motor's ability to maintain predictable and reliable motion over repeated cycles, further confirming its suitability for precision positioning applications.

The electrical efficiency of the driver circuit and the mechanical efficiency of the inchworm motor have been calculated to be 42 % and 29 % respectively. These actuators provide high resolution, submicron-level control, and several advantages over conventional electric motors, such as high blocking force, compact design, customizable geometry, and immunity to electromagnetic interference. These features make the motor particularly suitable for demanding industrial applications requiring precise and repeatable motion control.

Table 4
Comparative analysis of the proposed IM with previous reported work.

Parameters	Motor [50]	Motor [51]	Motor [52]	Motor [53]	Motor [54]	Motor [55]	Motor [29]	Motor [40]	Motor [56]	Motor [57]	Proposed IM
Driving voltage [V]	100	100	100	120	100	80	110	80	140	150	80–90
Operating frequency [Hz]	200	500	415	50	320	650	600	160	150	19	50–3000
Maximum speed [mm/s]	5.4	5.96	18.84	0.72	20	44.69	3.6	8.2	43.8	0.174	60
Maximum thrust force/ Load [N]	8.8	3	3.52	N/A	150	0.6	0.0007	0.5	3	8.6	4.41
No of piezo actuators	4	NA	NA	3	3	6	4	3	2	2	3
Efficiency [%]	NA	NA	2.07	Low	NA	Low	17	18.5	NA	NA	29
Travel range[mm]	20	0.12	0.42	11	NA	4.3	0.06	NA	25	NA	200
Self-locking at rest [Y/N]	Y	N	N	N	N	N	N	Y	N	Y	Y
Type of Piezo Motor	Piezo-IM	Stick-slip	Stick–slip	IM	IM	IM	IM	IM	IM	IM	IM
Volume [cm^3]	658.38	NA	NA	202.5	100.98	116.6	NA	262.5	NA	37.8	44.72

CRediT authorship contribution statement

Sandip Jana: Writing – original draft, Software, Resources, Data curation, Conceptualization. **Sofiane Ghenna:** Writing – review & editing, Validation, Investigation, Formal analysis. **Saikat Kumar Shome:** Writing – review & editing, Supervision, Investigation. **Yves Bernard:** Validation, Supervision, Investigation, Conceptualization. **Arup Kumar Nandi:** Visualization, Validation, Formal analysis, Data curation. **Laurent Daniel:** Supervision, Methodology, Investigation, Funding acquisition, Conceptualization.

Data availability

No datasets were generated or analyzed during the current study.

Funding

The authors gratefully acknowledge the funding received from the Indo French Center for the Promotion of Advanced Research (IFCPAR/CEFIPRA) for carrying out this work.

Conflict of interest

All authors declare no conflict of interest.

Acknowledgment

The authors gratefully acknowledge collaboration between CSIR-India, Centrale Supelec and Faurecia funded by the Indo-French Centre for the Promotion of Advanced Research (IFCPAR/CEFIPRA) under the grant number IFC71123 and S.J thanks CSIR HRDG, India for providing CSIR-SRF fellowship to carry out his research work with grant number 31/0019(11388)/2021-EMR-I.

Appendix

The simulink model parameters of the inchworm motor are considered as: $C_{c1} = 1.56$ kN/m; $k_{c1} = 25 \times \exp(6)$ N/m; K = 1000 N/m; $C_{c2} = 1.56$ kN/m; $k_{c2} = 25 \times \exp(6)$ N/m; d = 443 × exp(-12); $m_{c1} = 0.07$ kg; $m_e = 0.059$ kg; $m_{c2} = 0.07$ kg; $F_{pmax} = 1250$ N and maximum clamping force is considered as 5 N and frictional coefficient(μ) = 0.31.

References

[1] Shafik M, Shehab EM, Abdalla HS. A linear piezo-electric ultrasonic motor using a single flexural vibrating bar for electro-discharge system industrial applications. Int J Adv Manuf Technol 2009;45:287. https://doi.org/10.1007/s00170-009-1955-5.
[2] Tai M, Hingwe P, Tomizuka M. Modeling and control of steering system of heavy vehicles for automated highway systems. In: IEEE/ASME transactions on mechatronics, vol. 9; Dec. 2004. p. 609–18. https://doi.org/10.1109/Tmech.2004.839047. 4.
[3] Li Z, Zhu R, Yi X, Dong S. A high-power-density piezoelectric actuator operating in bicycling movement mechanism. In: IEEE transactions on industrial electronics, vol. 70; 2022. p. 6090–609. https://doi.org/10.1109/TIE.2022.3190900. 6.
[4] Delibas B, Koc B. A method to realize low velocity movability and eliminate friction induced noise in piezoelectric ultrasonic motors. In: IEEE/ASME transactions on mechatronics, vol. 25; Dec. 2020. p. 2677–87. https://doi.org/10.1109/TMECH.2020.2984367. 6.
[5] Taleb R, Seddiki L, Guelton K, Akdag H. Merging fuzzy observer-based state estimation and database classification for fault detection and diagnosis of an actuated seat. 2017 IEEE international conference on fuzzy systems. Naples, Italy: FUZZ-IEEE); 2017. p. 1–6. https://doi.org/10.1109/FUZZ-IEEE.2017.8015626.
[6] Zyner A, Worrall S, Nebot E. A recurrent neural network solution for predicting driver intention at unsignalized intersections. In: IEEE robotics and automation letters, vol. 3; July 2018. p. 1759–64. https://doi.org/10.1109/LRA.2018.2805314. 3.
[7] Jana S, Shome SK, Mukherjee A. Polynomial-based stability analysis of modified IMC-PID controller for piezoelectric actuator system in time delay environment. IETE J Res 2021;69(9):6210–23. https://doi.org/10.1080/03772063.2021.1987996.
[8] Ghenna S, Giraud F, Giraud-Audine C, Amberg M. Vector control of piezoelectric transducers and ultrasonic actuators. In: IEEE transactions on industrial electronics, vol. 65; June 2018. p. 4880–8. https://doi.org/10.1109/TIE.2017.2784350.
[9] Guo D, Nagel WS, Clayton GM, Leang KK. Spatial-temporal trajectory redesign for dual-stage nanopositioning systems with application in AFM. In: IEEE/ASME transactions on mechatronics, vol. 25; April 2020. p. 558–69. https://doi.org/10.1109/Tmech.2020.2971755.
[10] Liu X, et al. Vortex-driven rotation for three-dimensional imaging under microscopy. In: IEEE transactions on nanotechnology, vol. 17; July 2018. p. 688–91. https://doi.org/10.1109/Tnano.2018.2811958.
[11] Wlodarczyk KL, Bryce E, Schwartz N, et al. Scalable stacked array piezoelectric deformable mirror for astronomy and laser processing applications. Rev Sci Instrum 2014;85:024502. https://doi.org/10.1063/1.4865125.
[12] Galaktionov I, Sheldakova J, Samarkin V, Toporovsky V, Kudryashov A. Atmospheric turbulence with Kolmogorov spectra: software simulation, real-time reconstruction and compensation by means of adaptive optical system with bimorph and stacked-actuator deformable mirrors. Photonics 2023;10:1147. https://doi.org/10.3390/photonics10101147.
[13] Maksymova I, Greiner P, Wiesmeier J, Darrer F, Druml N. A MEMS mirror driver ASIC for beam-steering in scanning MEMS-based LiDAR. Proc. SPIE 11107, Laser Beam Shaping XIX 9 September 2019:111070C. https://doi.org/10.1117/12.2528312.
[14] Qin Y, Tian Y, Zhang D, Shirinzadeh B, Fatikow S. A novel direct inverse modeling approach for hysteresis compensation of piezoelectric actuator in feedforward applications. In: IEEE/ASME transactions on mechatronics, vol. 18; June 2013. p. 981–9. https://doi.org/10.1109/TMECH.2012.2194301. 3.
[15] Rakotondrabe M. Bouc–wen modeling and inverse multiplicative structure to compensate hysteresis nonlinearity in piezoelectric actuators. In: IEEE transactions on automation science and engineering, vol. 8; April 2011. p. 428–31. https://doi.org/10.1109/TASE.2010.2081979. 2.
[16] Shome SK, Jana S, Mukherjee A, Bhattacharjee P. Design of adaptive voltage dither control framework based on spectral analysis for nonlinear piezoelectric actuator. J Control Autom Electr Syst 2019;30. https://doi.org/10.1007/s40313-019-00506-6954–969.
[17] Shome SK, Jana S, Mukherjee A, Bhattacharjee P, Datta U. Bio inspired modified internal model control approach for improved disturbance rejection of piezo micro manipulator. In: Studies in informatics and control, vol. 27; 2018. p. 295–306. https://doi.org/10.24846/v27i3y201805. ISSN 1220-1766, 3.
[18] Locher GL. Micrometric linear actuator, vol. 296. Patent #3; 1967. p. 467.
[19] Tian X, Quan Q, Wang L, Su Q. An inchworm type piezoelectric actuator working in resonant state. In: IEEE access, vol. 6; 2018. p. 18975–83.
[20] Neill O, et al. Electromotive actuator. 1980. U.S. patent number 4,219,755, August 26.
[21] Lee S, Esashi M. Design of the electrostatic linear micro actuator based on the inchworm motion. Mechatronics 1995;5(8):963–72. https://doi.org/10.1016/0957-4158(95)00059-E.
[22] Vaughan M, Leo DJ. Integrated piezoelectric linear motor for vehicle applications. ASME international adaptive structures and materials systems symposium november 17-22. 2002. 10.1115/IMECE2002-32942.
[23] Tenzer PE, Mrad RB. A systematic procedure for the design of piezoelectric inchworm precision positioners. In: IEEE/ASME transactions on mechatronics, vol. 9; June 2004. p. 427–35. https://doi.org/10.1109/TMECH.2004.828627. 2.
[24] Canfield S, Edinger B, Frecker M, Koopmann G. Design of piezoelectric inchworm actuator and compliant end-effectors for minimally invasive surgery. SPIE Proceedings 1999;3668:835–43. https://doi.org/10.1117/12.350759.
[25] Galante T, et al. Design, modeling, and performance of a high force piezoelectric Inchworm motor. J Intell Mater Syst Struct 1999;10(12):962–72. https://doi.org/10.1106/21LN-RUYY-35CH-C1FD.
[26] Cho N, Jang W. The design and characterization of a Piezo-driven Inch- worm linear motor with a reduction-lever mechanism. JSME Int J Ser C 2004;47(3):803–11. https://doi.org/10.1299/jsmec.47.803.
[27] Moon C, et al. A new fast Inchworm type actuator with the robust I/Qheterodyne interferometer feedback. Mechatronics 2006;16(2):105–10. https://doi.org/10.1016/j.mechatronics.2005.10.003.
[28] Salisbury SP, Mrad RB, Waechter DF, Prasad SE. Characterization of a piezoworm stage. In: 2007 IEEE/ASME international conference on advanced intelligent mechatronics; 2007. p. 1–5. https://doi.org/10.1109/AIM.2007.4412444.
[29] Penskiy I, Gerratt AP, Bergbreiter S. Efficient electrostatic inchworm motors with simple control and high force density, 16th International Solid-State Sensors.

Actuators and microsystems conference. 2011, 2011. p. 2438–41. https://doi.org/10.1109/Transducers.2011.5969660.
[30] Ma L, Jiang C, Xiao J, Wang K, Xie W, Liu B. A piezoelectric Inchworm actuator based on the principle of flexible amplification. In: 2013 international conference on manipulation, manufacturing and measurement on the nanoscale; 2013. p. 201–6. https://doi.org/10.1109/3M-NANO.2013.6737414.
[31] Wang S, Rong W, Wang L, Sun L. Design, analysis and experimental performance of a stepping type piezoelectric linear actuator based on compliant foot driving. Smart Mater Struct 2016;25:115003. https://doi.org/10.1088/0964-1726/25/11/115003.
[32] Sun M, et al. Research on a novel non-resonant piezoelectric linear motor with lever amplification mechanism. Sensor Actuator 2017;261:302–10. https://doi.org/10.1016/j.sna.2017.04.030.
[33] Siyan S, Shao S, Xu M, Shao Y, Tian Z, Feng B. Piezoelectric inchworm rotary actuator with high driving torque and self-locking ability. Sensor Actuator Phys 2018;282:174–82. https://doi.org/10.1016/j.sna.2018.08.048.
[34] Tahmasebipour M, Sangchap M. A novel high performance integrated two-axis Inchworm piezoelectric motor. Smart Mater Struct 2019;29(1):015034. https://doi.org/10.1088/1361-665X/ab545e.
[35] Dong H, Li T, Wang Z, Ning Y. Design and experiment of a piezoelectric actuator based on Inchworm working principle. Sensor Actuator 2020;306:111950. https://doi.org/10.1016/j.sna.2020.111950.
[36] Wang R, Hu Y, Shen D, Ma J, Li J, Wen J. A novel piezoelectric inchworm actuator driven by one channel direct current signal. IEEE Trans Ind Electron March 2021; 68:2015–23. 10.1109/TIE.2020.2975493.
[37] Cai J, Chen F, Lining S, Dong W. Design of a linear walking stage based on two types of piezoelectric actuators. Sensor Actuator 2021;332:112067. https://doi.org/10.1016/j.sna.2020.112067.
[38] Yanling T, Zhichen H, Fujun W, et al. A novel friction-actuated 2-DOF high precision positioning stage with hybrid decoupling structure. Mech Mach Theor 2022;167:104511. https://doi.org/10.1016/j.mechmachtheory.2021.104511.
[39] Shubao S, Siyang S, Yan S, Minglong X. Long-range piezoelectric actuator with large load capacity using Inchworm and stick–slip driving principles. Precis Eng 2022;75:167–79. https://doi.org/10.1016/j.precisioneng.2022.02.007.
[40] Ling J, Chen L, Feng Z, Zhu Y. Development and test of a high speed pusher-type inchworm piezoelectric actuator with asymmetric driving and clamping configuration, Mech Mach Theor, Volume 176, 2022, 104997, ISSN 0094-114X, doi.org/10.1016/j.mechmachtheory.2022.104997.
[41] Ghenna S, Bernard Y, Daniel L. Design and experimental analysis of a high force piezoelectric linear motor. Mechatronics Feb. 2023;89:102928. https://doi.org/10.1016/j.mechatronics.2022.102928.
[42] https://innovationspace.ansys.com/product/fea-analysis-of-the-finite-element-method.
[43] Shome SK, Jana S, Bhattacharjee P. On learning-based approaches in power electronics engineering curriculum: a high switching inchworm motor drive case study. Comput Appl Eng Educ 2020;28(4). https://doi.org/10.1002/cae.22258.
[44] http://www.noliac.com/products/actuators/.
[45] https://www.ctscorp.com/Product-Series/NAC2022-H14.htm.
[46] https://www.ctscorp.com/Product-Series/NAC2021-H16.htm.
[47] Karnoop D. Computer simulation of stick-slip friction in mechanical dynamic systems. ASME J Dynam Syst, Measur Control 1985;107(1):100–3. https://doi.org/10.1115/1.3140698.
[48] Uchino K. Piezoelectric actuators and ultrasonic motors. Dordrecht: Kluwer Academic publishers; 1997. https://doi.org/10.1007/978-1-4613-1463-9.
[49] Xu Q, Li Y. Dahl model-based hysteresis compensation and precise positioning control of an XY parallel micromanipulator with piezoelectric actuation, Journal of Dynamic System. Measur Control 2010;132(4):41011. https://doi.org/10.1115/1.400171.
[50] Mohammad T, Salisbury SP. Design and assessment of a Z-Axis precision positioning stage with centimeter range based on a piezoworm motor. In: IEEE/ASME transactions on mechatronics, vol. 20; Oct. 2015. p. 2021–30. https://doi.org/10.1109/TMECH.2014.2360644. 5.
[51] Cheng T, He M, Li H, Lu X, Zhao H, Gao H. A novel trapezoid-type stick–slip piezoelectric linear actuator using right circular flexure hinge mechanism. In: IEEE transactions on industrial electronics, vol. 64; July 2017. p. 5545–52. https://doi.org/10.1109/TIE.2017.2677318. 7.
[52] Zhang X, Yu Y, Gao Q, Qiao G, Li Z, Lu X, Cheng T. A stick-slip linear piezoelectric actuator with mode conversion flexible hinge driven by symmetrical waveform. Smart Mater Struct 2020;29(5):055035. https://doi.org/10.1088/1361-665X/ab7f42.
[53] Dong H, Li T, Wang Z, Ning Y. Design and experiment of a piezoelectric actuator based on inchworm working principle. Sensor Actuator 2020;A:111950. https://doi.org/10.1016/j.sna.2020.111950.
[54] Tenzer PE, Mrad RB. A systematic procedure for the design of piezoelectric inchworm precision positioners. In: IEEE/ASME transactions on mechatronics, vol. 9; June 2004. p. 427–35. https://doi.org/10.1109/Tmech.2004.828627. 2.
[55] Guo He L, Zhang Q, Liang Pan C, Ju B, Feng ZH. Piezoelectric motor based on synchronized switching control. Sensor Actuator Phys 2013;197:53–61. https://doi.org/10.1016/j.sna.2013.03.033. ISSN 0924-4247.
[56] Meng L, Yan P, Liu P. A high-speed inchworm piezoelectric actuator with multi-layer flexible clamping: design, modeling, and experiments. Mech Syst Signal Process 2024;218:111558. https://doi.org/10.1016/j.ymssp.2024.111558. ISSN 0888-3270.
[57] Liu L, Ji Z, Zhang Y, Chen H, Lou W, Kong M. A single-clamp inchworm actuator with two piezoelectric stacks. Micromachines 2024;15:718. https://doi.org/10.3390/mi15060718.

Sandip Jana received his BTech in Electrical Engineering and MTech degree in Power Electronics and Machine Drives from National Institute of Technology, Durgapur, India in 2017. He was a research fellow in Group of Electrical Engineering, CNRS-Centrale Supelec, UPSud, Paris and engaged as a Junior Research Fellow of an Indo French project (IFCPAR/CEFIPRA). After that he engaged two years as a CSIR-Senior Research Fellow (Direct) at CSIR-CMERI. Currently he is working as a PhD research scholar at AcSIR, India. His research interests include power electronics converters, piezo electric actuator system and motor control.

Sofiane Ghenna received Engineer's degree in Electrical Engineering in 2011 from National Polytechnic School of Algiers, Algeria and the Master's degree in Electrical Engineering Systems from National Polytechnic Institute - ENSEEIHT Toulouse, France, in 2012 and Ph.D degree in electrical engineering from Lille University, France, in 2016. After one year as Teaching and Research Assistant at Lille University, and two years as Post-Doctoral researcher at CentraleSupélec, Paris, France, he is currently Associate Professor at Université Polytechnique Hauts-de-France Valenciennes, France. His research interests include design, modeling and control of smart materials based actuators.

Saikat Kumar Shome is working as a Principal Scientist at CSIR CMERI Durgapur, a national R&D institute under Ministry of Science and Technology, Govt of India. He has done his BTech, followed by MTech in Mechatronics and PhD (Engg). He is also concurrently associated with AcSIR, An Institute of National Importance, Govt of India as an Associate Professor. His research areas include robotics, non-linear control and mechatronics.

Yves Bernard was born in Paris in France, on 1974. He graduated from the Paris-Saclay University with a diploma in energy transformation. He became a doctor in September 2000 with a thesis about the magnetic hysteresis modeling using finite element method. He was professor assistant at Paris-Saclay University since September 2001. His research activity was about the modeling and conception of piezoelectric devices. Since 2012, he is professor with a research topic on piezo motors.

Arup Kumar Nandi received B.E. degree in mechanical engineering from the National Institute of Technology, Durgapur, India, in 1995 and Ph.D. degree from the Indian Institute of Technology, Kanpur, India, in 2011. He is currently a Senior Principal Scientist with the Central Mechanical Engineering Research Institute (CSIR), Durgapur, India. His main research interests include neural networks, and evolutionary algorithms and its applications in engineering design.

Laurent Daniel received Ph.D. degree from Ecole Normale Supérieure de Cachan, Cachan, France, in 2003 and Habilitation degree in Physics from the Université Paris-Sud, Orsay, France, in 2011. Since 2015, he has been a Full Professor with Centrale Supélec, Université Paris-Saclay, Gif sur Yvette, France. His research activities are dedicated to electromechanical and magnetomechanical couplings in materials for electrical engineering applications and definition of multiscale methods for prediction of such coupled phenomena. Since 2014, he has been the Director of the Automotive Mechatronics Chair, a partnership between Centrale Supélec, Esigelec and automotive company Forvia.